Velocity Inversion by Global Optimization Using Finite-Offset Common-Reflection-Surface Stacking

Marcelo Jorge Luz Mesquita (UFPA) and João Carlos Ribeiro Cruz (UFPA)

Abstract

We developed a fully automatic P-wave velocity inversion methodology using pre-stack two-dimensional seismic data. It is performed in two steps, at first using image rays and an a priori known initial velocity model we determine the reflector interfaces in depth from the time-migrated section. The generated depth macro-model is used as input at the second step, where the parametrization of the velocity model is made layer by layer. The inversion strategy is based on the scan of semblance measurements in each common-midpoint gather guided by the Finite-Offset Common-Reflection-Surface traveltime paraxial approximations. For beginning the inversion in the second step, the finite-offset common-midpoint central rays is built by ray tracing from the velocity macro-model obtained in the first step. By using the arithmetic mean of total semblance calculated from the whole common-midpoint gathers as objective function, layer after layer, a global optimization method called Very Fast Simulated Annealing algorithm is applied in order to obtain the convergence of the objective function toward the global maximum. By applying to synthetic and real data, we showed the robustness of the inversion algorithm for yielding an optimized P-wave velocity macro-model from pre-stack seismic data.

Introduction

The estimate of an accurate velocity macro-model is an important stage of the seismic processing for providing a reliable seismic interpretation of the geological structures of interest to the oil and gas exploration. In recent years, we have seen an increasing application of the Full Waveform Inversion (FWI) method for estimating velocity model in complex geological environments (Tarantola, 1984; Virieux and Operto, 2009). Nevertheless, it is very sensitive to the chosen initial velocity model (Prieux et al, 2012). In this sense, the seismic tomography approaches continue being an essential alternative to start the accurate velocity inversion (Rawlinson et al, 2010).

Since eighty years, the coherency measurements have been used for building efficient velocity inversion strategies using global optimization (Landa et al., 1988; 1989). It has the advantage that does not depend on pre-stack time picking and does not use time data fitting.

Using coherency measurements and local optimization algorithm, Biondi (1992) developed an inversion algorithm based on the evaluation of the beam stack energy on CMP gathers, by searching for the velocity model that best predicts the reflection events in beam-stacked data. Prieux et al. (2012) estimated initial velocity models for FWI using the stereotomography, with application to synthetic and marine seismic data. Alternatively, the Normal-Incidence-Point (NIP) tomography has been applied for determining the initial model from short-spread seismic data for FWI (Köhn et al., 2016).

We start the proposed inversion strategy from seismic reflections interpreted on the time-migrated seismic section. Each interpreted horizon is depth converted by using an a priori known velocity model and image rays to respective interface. We build a fun of finite-offset central rays through the chosen layers for a set of CMP gathers along the model. By using the Finite-Offset Common-Reflection-Surface (FO CRS) traveltime approximation for each central ray, we build possible stack trajectories within given apertures (Jäger, 1999; Zhang et al, 2001; Garabito et al, 2001; Garabito et al, 2011). Guided by the FO CRS traveltime confined to the CMP gathers, we calculate the coherency measurements using the semblance as the objective function. Layer by layer, we carry out an optimization process by which we estimate the best interval velocities that maximize the semblance objective function by means a global search algorithm namely Very Fast Simulated Annealing (VFSA) (Ingber, 1989). By considering a probability criterion of the VFSA algorithm, the velocity is up to date even when the semblance has a relative low value.

By applying the proposed inversion strategy to synthetic and real data (Tacutu basin, in northern Brazil), we showed its very good performance by yielding an optimized P-wave interval velocity model from pre-stack seismic data, which are useful as initial guess for more sophisticated velocity inversion and migration methods.

Method

Modeling parametrization

Let X be the horizontal distance along the earth's surface, Z the depth, n the number of layers and m the number of nodepoints. Velocity within each layer can be assumed constant or vary laterally, where curved interfaces and lateral varying velocities are represented by spline functions (Landa et al., 1989). Unknown parameters for inversion are vertical node locations for interfaces and velocity values of each layer given by the vector of parameters $\mathbf{m} = \{\mathbf{Z}, \mathbf{V}\}$. The inversion algorithm is performed layer after layer and we may assume, or not,

that the number of nodepoints is the same for each layer (Landa et al., 1988; 1989). Figure 1 shows the interpretative model of the medium as previously described.

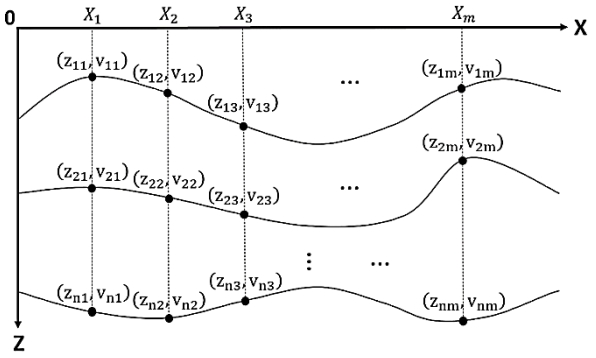

Figure 1: Scheme of model parametrization constituted by layers separated by curved and smooth interfaces. Velocity within each layer can be assumed constant or vary laterally.

Time-to-depth conversion

This process is described as follows: given a curve time-offset, corresponding to the reflections of a horizon in depth, find the position of the horizon and produce an image depth-offset. We obtain the traveltimes of the events from pickings into time migrated sections. These times are very important points for determining the depth using the image-ray tracing technique at each iteration (Hubral, 1977; Filpo et al, 2016). We convert the selected points in time to the respective positions in depth, according to the guessed velocity model, i.e. **Z** is a functional of **V**, and after that we interpolate using the method of cubic splines, resulting in the reflection interface layer model.

FO-CRS traveltime

For a central ray that starts at *S* with initial velocity v_S and start angle β_S, reflects at *R* in the subsurface, and emerges at the surface in *G* with final velocity v_G and emergence angle β_G, by considering $v_S = v_G = v_0$, the traveltime of the finite-offset paraxial ray, so-called finite-offset CRS stacking operator, is expressed by (Zhang *et al*. 2001):

$$T_{CRS}^2 = \left[t_0 + \left(\frac{1}{v_0}\right)(a_1\Delta x_m + a_2\Delta h)\right]^2 + \left(\frac{t_0}{v_0}\right)[a_3 - a_4]\Delta x_m^2 - \left(\frac{t_0}{v_0}\right)[a_4 - a_5]\Delta h^2 + 2\left(\frac{t_0}{v_0}\right)[a_4 + a_5]\Delta x_m \Delta h. \quad (1)$$

By considering the relationships: $a_1 = \sin\beta_G + \sin\beta_S$, $a_2 = \sin\beta_G - \sin\beta_S$, $K = 4K_1 - 3K_3$, $a_3 = K\cos^2\beta_G$, $a_4 = K_2\cos^2\beta_S$ and $a_5 = K_3\cos^2\beta_G$. Where, t_0 is the traveltime along the central ray, β_S and β_G are the start and emergence angles of the central ray in the position of the source *S* and the receiver *G* with coordinates x_S and x_G, respectively. The $\Delta x_m = x_m - x_0$ and $\Delta h = h - h_0$ correspond to the midpoint and half-offset displacements, where, $x_0 = (x_G + x_S)/2$ is the midpoint and $h_0 = (x_G - x_S)/2$ is the half-offset of the central ray with finite-offset. The midpoint x_m and the half-offset h are the coordinates of an arbitrary paraxial ray with finite-offset. The wave velocity at the source *S* and receiver *G* is given by v_S and v_G, respectively. The quantities K_1, K_2 and K_3 are the wavefront curvatures associated to the central ray and they are calculated in the respective emergence points (Garabito et al., 2011).

For CMP configuration, the source and receiver of the paraxial vicinity, $\bar{S}$ and $\bar{G}$ are located symmetrically in relation to their corresponding points *S* and *G*, in the central ray. Considering that the common midpoint is common to the central and paraxial rays, the CMP condition implies $\Delta x_m = 0$, and the FO CRS traveltime approximation becomes (Garabito et al, 2011):

$$T_{CMP}^2 = \left[t_0 + \left(\frac{1}{v_0}\right)(a_2\Delta h)\right]^2 - \left(\frac{t_0}{v_0}\right)[a_4 - a_5]\Delta h^2. \quad (2)$$

Inverse problem

The proposed method involves the application of various techniques, as shown in the flowchart of the Figure 2.

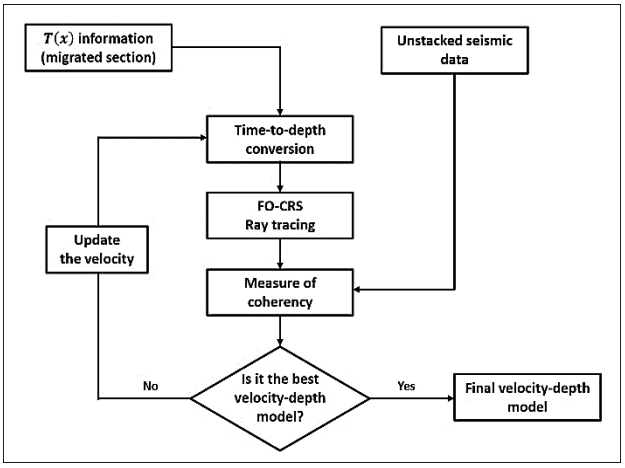

Figure 2: Flowchart showing the scheme of the proposed algorithm (adapted from Landa et al., 1989).

Starting from an initial depth-velocity model and from the very good interpreted migrated seismic section, we select all interested reflection time horizons. After, using image ray time-to-depth converter, we have an ensemble of model parameters represented by the vector $\mathbf{m} = \{\mathbf{Z}, \mathbf{V}\}$ that represents the velocity values and the interfaces of all layers presented in the depth model. The vector of interface nodes $\mathbf{Z} = \mathbf{Z}(\mathbf{V})$ is a function of the velocity vector in each layer. The optimum $\mathbf{m} = \{\mathbf{Z}, \mathbf{V}\}$ is obtained by finding the maximum coherency calculated for all pre-stack trace gathers in a time window along traveltime trajectories, layer after layer.

Let us adopt the semblance measurement (Neidell and Taner, 1971) to estimate the presence or absence of signals correlated along the traveltime curves calculated by FO-CRS approximation in the CMP gathers. The function S, that varies between 0 and 1, is given by:

$$S(\mathbf{m}) = \frac{\sum_t \left[\sum_{i=1}^{M} A_{i,t(i)}\right]^2}{M \sum_t \left[\sum_{i=1}^{M} A_{i,t(i)}^2\right]} \quad , \qquad (3)$$

where $\mathbf{m} = \{\mathbf{V}, \mathbf{Z}(\mathbf{V}), \mathbf{W}(\mathbf{V}, \mathbf{Z})\}$, with $\mathbf{W} = (\boldsymbol{K_2}, \boldsymbol{K_3}, \boldsymbol{\beta_S}, \boldsymbol{\beta_G})$, $\boldsymbol{A_{i,t(i)}}$ is the seismic signal amplitude indexed by the trace order number and stacking traveltime curve $\boldsymbol{t(i)}$, $\sum_{\boldsymbol{t}}$ is the time window for coherency measure and $\boldsymbol{M}$ is the number of traces in the CMP gather (pre-stacked section).

In our inverse process, for each layer, we use the arithmetic mean of all semblances values calculated as maximization parameter. Thus, equation (3) becomes:

$$E(\mathbf{m}) = \frac{1}{n} \sum_{j=1}^{n} \left[\frac{\sum_t \left[\sum_{i=1}^{M} A_{i,t(i)}\right]^2}{M \sum_t \left[\sum_{i=1}^{M} A_{i,t(i)}^2\right]} \right]_j \quad , \qquad (4)$$

where n is the number of CMP gathers analyzed. The nature of VFSA optimization algorithm (Ingber, 1989; 1993) is calculating the minimum energy value, so it is usual the multiplication of E by the factor (-1) so that its maximum amount is estimated.

Examples

Synthetic data

In this example, we applied our method to the model presented in Figure 3. This model consists of five homogeneous and isotropic layers, with velocities: $v_1 = 1507$ m/s, $v_2 = 1700$ m/s, $v_3 = 1900$ m/s, $v_4 = 2100$ m/s and $v_5 = 2300$ m/s. We analyzed eighteen CMP gathers per layer, spaced 500 m each. The first CMP gather is located at 737.5 m and the last one at 9237.5 m. Figure 4 shows the time-migrated section and the picked points to estimate the traveltimes of image-rays in the main events. Let us consider our initial model (Figure 5) by applying the time-depth conversion using the first-guess velocities, with the true interfaces shown in dashed lines.

Tables 1a and 1b show the results reached, where v represents the true velocity, v_i the first-guess velocity, v_{sr} the velocity search range, v_e the estimated velocity, e_v the percentage error related to velocity. For VFSA algorithm, T_0 indicates the initial temperature, c is the parameter that tunes the cooler rate and k is the annealing step, or iteration. For this example, we choose $T_0 = 2$ for all layers, $c = 0.2$ for layers 1 to 4 and $c = 0.3$ for layer 5. Figure 6 shows the final model specifying the estimated velocities in each layers and the exact interfaces by dashed lines. The results agree well with the exact model.

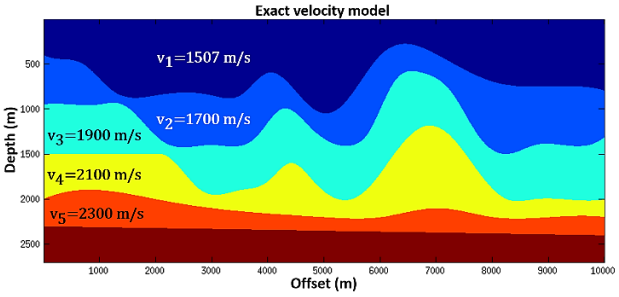

Figure 3: Geological model of seismic velocities.

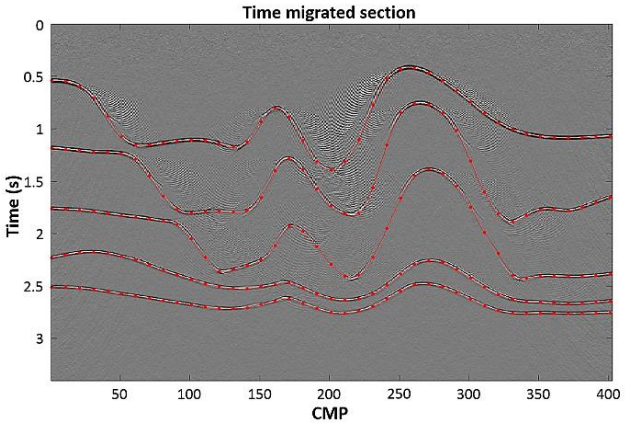

Figure 4: Time-migrated section and the picked points to estimate the traveltimes of image-rays in the main events.

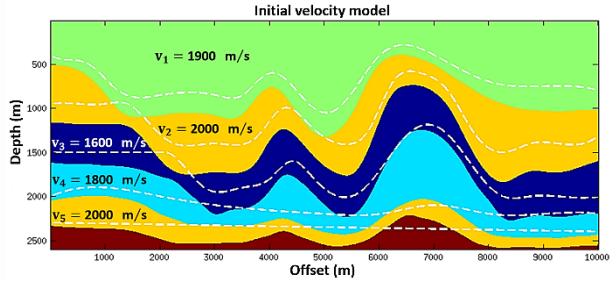

Figure 5: Initial model with first-guess velocities for synthetic data. Dashed lines represent the exact interfaces.

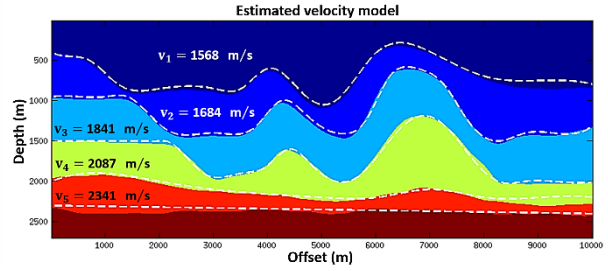

Figure 6: Estimated model for the synthetic data. The results agree well with the exact model. Dashed lines represent the exact interfaces.

Field data

We applied the proposed strategy to a field data that consists of part of the Tacutu Basin located on the northern border of Brazil and the Republic of Guyana. Figure 7 shows the time-migrated section where we interpreted seven dominant reflection events. This section comprises a horizontal distance of 10500 m and a time of 1.6 seconds. Input data in this case consists of 39 CMP gathers, where the first (CMP 1020) is located at 500 m and the last (CMP 1400) at 10000 m. We applied the Dix formulae to stacking velocities and times picked to define the search range and initial guesses for each layer. Figure 8 shows the velocity model for these initial guesses. The evaluation nodes in the model match the picking points in migrated section, located between 0 and 10500 m, and spaced by 1750 m each. We

consider the source and geophone of FO CRS central-ray placed 500 m from the mid-point.

Table 1a: Parameters and results of the inverse algorithm applied to synthetic case for layers 1, 2 and 3.

	Layer 1	Layer 2	Layer 3
$\mathbf{v}\ (\mathbf{m/s})$	1507	1700	1900
$\mathbf{v_i}\ (\mathbf{m/s})$	1900	2000	1600
$\mathbf{v_{sr}}\ (\mathbf{m/s})$	[1400; 2000]	[1600; 2100]	[1600; 2100]
$\boldsymbol{k}$	200	100	100
$\boldsymbol{E}$	0.3475	0.3481	0.3755
$\mathbf{v_e}\ (\mathbf{m/s})$	1568	1682	1841
$\mathbf{e_v}\ (\%)$	4.04	1.06	3.10

Table 1b: Parameters and results of the inverse algorithm applied to synthetic case for layers 4 and 5.

	Layer 4	Layer 5
$\mathbf{v}\ (\mathbf{m/s})$	2100	2300
$\mathbf{v_i}\ (\mathbf{m/s})$	1800	2000
$\mathbf{v_{sr}}\ (\mathbf{m/s})$	[1800; 2200]	[2000; 2500]
$\boldsymbol{k}$	100	100
$\boldsymbol{E}$	0.1924	0.3690
$\mathbf{v_e}\ (\mathbf{m/s})$	2087	2341
$\mathbf{e_v}\ (\%)$	0.62	1.78

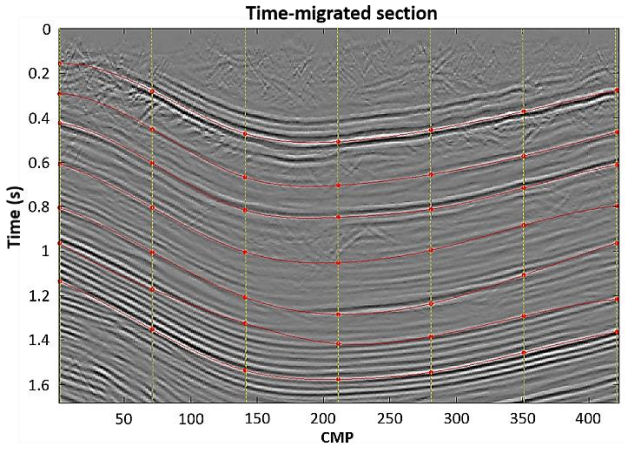

Figure 7: Time-migrated section for field data.

Tables from 2a to 2g show the results of the inverse scheme. We choose $T_0 = 2$ for all layers, $c = 0.1$ for layer 1 and $c = 0.3$ for the remaining layers. An example of a CMP gather, at 1250 m, and the FO CRS traveltime curve for semblance evaluation related to reflection event in layer 7 is shown in Figure 9. Figure 10 shows the final velocity-depth model after applying the algorithm.

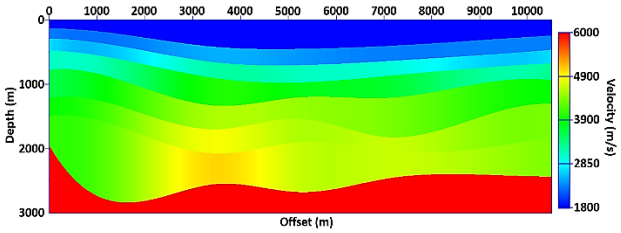

Figure 8: Initial velocity-depth model with first guesses for the field data.

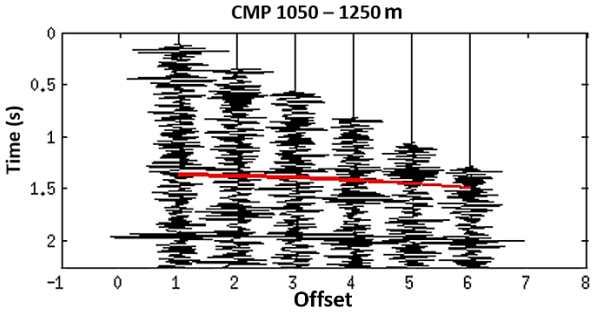

Figure 9: CMP gather and FO-CRS traveltime curve for semblance evaluation related to layer 7.

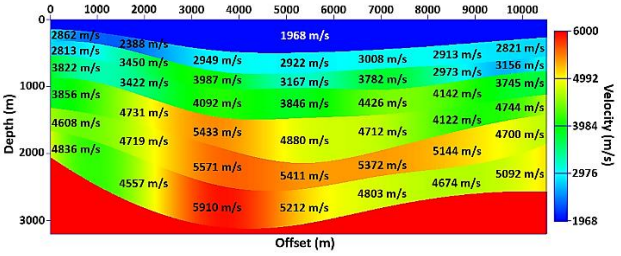

Figure 10: Velocity-depth model showing estimated velocities in specified points represented by spline functions.

Table 2a: Parameters and results of the inverse algorithm applied to field data: layer 1.

	Layer 1
$\mathbf{v_i}\ (\mathbf{m/s})$	1800
$\mathbf{v_{sr}}\ (\mathbf{m/s})$	[1900; 2700]
$\boldsymbol{k}$	400
$\boldsymbol{E}$	0.2046
$\mathbf{v_e}\ (\mathbf{m/s})$	1968

Table 2b: Parameters and results of the inverse algorithm applied to field data: layer 2.

	Layer 2
$\mathbf{v_i}$ $(\mathbf{m/s})$	[2300, 2300, 2500, 2400, 2300, 2300, 2300]
$\mathbf{v_{sr}}$ $(\mathbf{m/s})$	[2300, 2300, 2500, 2400, 2300, 2300, 2300; 3200, 3200, 3400, 3300, 3200, 3200, 3200]
$\boldsymbol{k}$	500
$\boldsymbol{E}$	0.2256
$\mathbf{v_e}$ $(\mathbf{m/s})$	[2862, 2388, 2949, 2922, 3008, 2913, 2821]

Table 2c: Parameters and results of the inverse algorithm applied to field data: layer 3.

	Layer 3
$\mathbf{v_i}$ $(\mathbf{m/s})$	[2700, 2700, 3200, 3100, 3000, 2700, 2700]
$\mathbf{v_{sr}}$ $(\mathbf{m/s})$	[2700, 2700, 3200, 3100, 3000, 2700, 2700; 3600, 3600, 4100, 4000, 3900, 3600, 3600]
$\boldsymbol{k}$	400
$\boldsymbol{E}$	0.2193
$\mathbf{v_e}$ $(\mathbf{m/s})$	[2813, 3450, 3987, 3167, 3782, 2973, 3156]

Table 2d: Parameters and results of the inverse algorithm applied to field data: layer 4.

	Layer 4
$\mathbf{v_i}$ $(\mathbf{m/s})$	[3100, 3400, 4000, 3800, 3700, 3300, 3300]
$\mathbf{v_{sr}}$ $(\mathbf{m/s})$	[3100, 3400, 4000, 3800, 3700, 3300, 3300; 4000, 4300, 4900, 4700, 4600, 4200, 4200]
$\boldsymbol{k}$	400
$\boldsymbol{E}$	0.2131
$\mathbf{v_e}$ $(\mathbf{m/s})$	[3822, 3422, 4092, 3846, 4426, 4142, 3745]

Table 2e: Parameters and results of the inverse algorithm applied to field data: layer 5.

	Layer 5
$\mathbf{v_i}$ $(\mathbf{m/s})$	[3600, 4100, 4600, 4500, 4400, 4100, 3900]
$\mathbf{v_{sr}}$ $(\mathbf{m/s})$	[3600, 4100, 4600, 4500, 4400, 4100, 3900; 4500, 5000, 5500, 5400, 5300, 5000, 4800]
$\boldsymbol{k}$	400
$\boldsymbol{E}$	0.2223
$\mathbf{v_e}$ $(\mathbf{m/s})$	[3856, 4731, 5433, 4880, 4712, 4122, 4744]

Table 2f: Parameters and results of the inverse algorithm applied to field data: layer 6.

	Layer 6
$\mathbf{v_i}$ $(\mathbf{m/s})$	[3900, 4400, 4900, 4600, 4700, 4500, 4400]
$\mathbf{v_{sr}}$ $(\mathbf{m/s})$	[3900, 4400, 4900, 4600, 4700, 4500, 4400; 4800, 5300, 5800, 5500, 5600, 5400, 5300]
$\boldsymbol{k}$	300
$\boldsymbol{E}$	0.2445
$\mathbf{v_e}$ $(\mathbf{m/s})$	[4608, 4719, 5571, 5411, 5372, 5144, 4700]

Table 2g: Parameters and results of the inverse algorithm applied to field data: layer 7.

	Layer 7
$\mathbf{v_i}$ $(\mathbf{m/s})$	[4100, 4500, 5100, 4700, 4700, 4600, 4400]
$\mathbf{v_{sr}}$ $(\mathbf{m/s})$	[4100, 4500, 5100, 4700, 4700, 4600, 4400; 5000, 5400, 6000, 5600, 5600, 5500, 5300]
$\boldsymbol{k}$	300
$\boldsymbol{E}$	0.2229
$\mathbf{v_e}$ $(\mathbf{m/s})$	[4836, 4557, 5910, 5212, 4803, 4674, 5092]

Conclusions

We have presented a 2-D methodology based on the coherency inversion method, which consists to maximize a semblance function calculated from pre-stack seismic data in order to obtain information about the velocities in the subsurface. Our approach consists in application of the FO-CRS approximation and VFSA algorithm in order to estimate the best velocity-depth model. The FO-CRS method was suitable for calculations required in the semblance maximization and in the optimization process. The VFSA algorithm has showed to be very efficient solving this kind of problems and it is practically independent of initial model. The method has been successfully tested on synthetic data agreeing very well with exact model, as well as to the field data.

Acknowledgments

The authors would like to thank the *Programa de Pós-graduação em Geofísica – Universidade federal do Pará*, Geophysical network of PETROBRAS, and CAPES for the support.

References

Biondi, B. Velocity estimation by beam stack. Geophysics, v. 54, p. 1012-1025, 1992.

Filpo, E.; Portugal, R.; Zago, N.; Cunha, P. M.; Vicentini, A.; Carbonesi, J. L. Image-ray concept as the key to 20 years of success of time-to-depth conversion in Petrobras. The Leading Edge, abril, 2016.

Garabito, G.; Cruz, J. C. R., Hubral, P., Costa, J., 2001, Common reflection surface stack by global optimization. 71th SEG Meeting. Extended Abstracts.

Garabito, G.; Oliva, P. C.; Cruz, J. C. R., 2011, Numerical analysis of the finite-offset common-reflection-traveltime approximations. Journal of Applied Geophysics, n. 74, p. 89-99.

Hubral, P., 1977, Time migration – Some ray theoretical aspects: Geophysical Prospecting, 25, 738-745.

Ingber, L., 1989, Very fast simulated reannealing. Mathl. Comput. Modeling 12(8), 967-993.

Ingber, L., 1993, Simulated annealing: Practice versus theory. Mathl. Comput. Modeling 18(11), 29-57.

Jäger, R., 1999, The common-reflection-surface stack-theory and application. Master's thesis. Universität Karlsruhe (Germany).

Köhn, D.; Nil, D.; Rabbel, W. Estimation of long-wavelength initial models for seismic full waveform inversion – Part 2 CRS-Stack and NIP-wave tomography. 76th annual meeting of the German Geophysical Society (DGG), 2016.

Landa, E.; Kosloff, D.; Keydar, S.; Koren, Z.; Reshef, M., 1988, A method for determination of velocity and depth from seismic reflection data. Geophysical Prospecting, 36, p. 223-243.

Landa, E.; Beydoun, W.; Tarantola, A., 1989, Reference velocity model estimation from prestack waveforms: Coherency optimization by simulated annealing. Geophysics, v.54, n. 8, p. 984-990.

Neidell, N. S.; Taner, M. T., 1971, Semblance and other coherency measures for multichannel data. Geophysics, v. 36, p. 482-497.

Prieux, V.; Lambarè, G.; Operto, S.; Virieux, J. Building starting models for full waveform inversion from wide-aperture data by stereotomography. Geophysical Prospecting, p. 1-29, 2012.

Rawlinson, N., Pozgay, S., Fishwick, S., 2010, Seismic tomography: A window into deep Earth. Physics of the Earth and Planetary interiors, v. 178, p. 101-135.

Tarantola, A., 1984, Inversion of seismic reflection data in the acoustic approximation. Geophysics, v. 49, p. 1259-1266.

Virieux, J., and Operto, S., 2009, An overview of full-waveform inversion in exploration geophysics. Geophysics, v. 74, n. 6, p. WCC1-WCC26.

Zhang, Y.; Bergler, S.; Tygel, M.; Hubral, P., 2001, Common-Reflection-Surface (CRS) stack for common-offset. Geophy. Prospect. 49, 709-718.